CHEMISTRY OF MATERIALS
Article

Chem. Mater. **2009,** *21,* 5397–5405 5397
DOI:10.1021/cm901885c

Morphology Diagram of a Diblock Copolymer−Aluminosilicate Nanoparticle System

Benjamin C. Garcia,[†,∥] Marleen Kamperman,[†,⊥] Ralph Ulrich,[†,#] Anurag Jain,[†,▽] Sol M. Gruner,[‡,§] and Ulrich Wiesner*[,†]

[†]*Department of Materials Science and Engineering and* [‡]*Department of Physics and* [§]*Cornell High Energy Synchrotron Source (CHESS), Cornell University, Ithaca, New York 14853.* [∥]*Present address: Hewlett-Packard IPG R&D, 16399 W Bernardo Drive, MS 61U66, San Diego, CA 92127.* [⊥]*Present address: Leibniz Institute for New Materials, Campus D2 2, 66123 Saarbrücken, Germany.* [#]*Present address: Lanxess Deutschland GmbH, Gebaüde G17, 41539 Dormagen, Germany.* [▽]*Present address: Intel Corporation, 5200 NE Elam Young Parkway, RA3-335, Hillsboro, OR 97124.*

Received June 30, 2009. Revised Manuscript Received September 23, 2009

We explore the morphology space of nanocomposites prepared from poly(isoprene-*block*-ethylene oxide) (PI-*b*-PEO) diblock copolymers as structure directing agents for aluminosilicate nanoparticles prepared from (3-glycidyloxypropyl)trimethoxysilane (GLYMO) and aluminum(III) *sec*-butoxide. The results of structural investigations of over 60 polymer−inorganic nanocomposites are reported. They are obtained from 12 different block copolymers of varying molecular weight (∼10−100 kg/mol) and PEO weight fraction ($f_w \sim 0.1-0.8$) through addition of different amounts of inorganic components. Eight different morphologies as well as composites with biphasic character are observed. Individual block copolymers show up to five different well-defined morphologies upon addition of the inorganic sols. Differential scanning calorimetry (DSC) studies on the composites show that the addition of the inorganic components suppresses PEO crystallization when the inorganic to PEO weight fraction ratio of the composites is greater than 1.3−1.5. The eight phases are mapped out using two- and three-component morphology diagrams.

Introduction

A wide variety of biomaterials and other soft materials have astonishingly rich phase behavior characterized by periodically ordered structures observed as a consequence of competing interactions (hydrogen bonding, electrostatics, van der Waals forces, etc.). In recent years increasing efforts have been made to transfer this structure control to inorganic materials. An example of such a system is the template based sol−gel synthesis of organic−inorganic nanocomposites using ionic surfactants offering a wide range of new and useful materials with controlled architectures.[1,2] Similarly, amphiphilic block copolymers have been shown to direct the structure of silica into a variety of mesophases by using the interactions between the silicate source and the organic amphiphile.[3−6] In the meantime this approach has been applied to nonoxide type ceramics, crystalline oxides, and metals.[7−9] Full control over morphology in multiphase systems is a fascinating challenge in research since it is a key step in controlling the material's mechanical, optical, electronic, and ionic properties. Here, we map the morphology space of a linear amphiphilic block copolymer blended with organically modified aluminosilicate nanoparticles prepared from a sol−gel approach. The resulting organic−inorganic nanocomposites exhibit eight different mesostructures comprising morphologies known and unknown in pure block copolymer systems. Nanocomposites with compositions near the boundary between two different morphologies show biphasic character adopting the structure of both neighboring morphologies. Phase diagrams have been prepared by various groups using block copolymers and organic additives (solvents, epoxy, and other polymers),[10−13] but this is

*To whom correspondence should be addressed. E-mail: ubw1@cornell.edu.

(1) Kresge, C. T.; Leonowicz, M. E.; Roth, W. J.; Vartuli, J. C.; Beck, J. S. *Nature* **1992**, *359*, 710–712.
(2) Raman, N. K.; Anderson, M. T.; Brinker, C. J. *Chem. Mater.* **1996**, *8*, 1682–1701.
(3) Bagshaw, S. A.; Prouzet, E.; Pinnavaia, T. J. *Science* **1995**, *269*, 1242–1244.
(4) Templin, M.; Franck, A.; DuChesne, A.; Leist, H.; Zhang, Y. M.; Ulrich, R.; Schadler, V.; Wiesner, U. *Science* **1997**, *278*, 1795–1798.
(5) Zhao, D. Y.; Feng, J. L.; Huo, Q. S.; Melosh, N.; Fredrickson, G. H.; Chmelka, B. F.; Stucky, G. D. *Science* **1998**, *279*, 548–552.
(6) Göltner, C. G.; Henke, S.; Weissenberger, M. C.; Antonietti, M. *Angew. Chem., Int. Ed.* **1998**, *37*, 613–616.
(7) Kamperman, M.; Garcia, C. B. W.; Du, P.; Ow, H. S.; Wiesner, U. *J. Am. Chem. Soc.* **2004**, *126*, 14708–14709.
(8) Lee, J.; Orilall, M. C.; Warren, S. C.; Kamperman, M.; DiSalvo, F. J.; Wiesner, U. *Nat. Mater.* **2008**, *7*, 222–228.
(9) Warren, S. C.; Messina, L. C.; Slaugther, L. S.; Kamperman, M.; Zhou, Q.; Gruner, S. M.; DiSalvo, F.; Wiesner, U. *Science* **2008**, *320*, 1748–1752.
(10) Lai, C.; Russel, W. B.; Register, R. A. *Macromolecules* **2002**, *35*, 841–849.
(11) Alexandridis, P.; Olsson, U.; Lindman, B. *Langmuir* **1998**, *14*, 2627–2638.

Published on Web 10/20/2009

the first time, to the best of our knowledge, that a comprehensive mesostructural morphology space is mapped using inorganic nanoparticles as the swelling component.

The unique morphology space of the block copolymer−aluminosilicate nanoparticle system is mapped by varying two parameters: block copolymer composition and inorganic content. Our approach induces changes in morphology by selectively swelling one of the blocks of an amphiphilic diblock copolymer with sol−gel based inorganic nanoparticles.[14] The diblock copolymer is poly(isoprene-*b*-ethylene oxide), PI-*b*-PEO, and the sol−gel precursors are a mixture of an organically modified silane, (3-glycidyloxypropyl)trimethoxysilane (GLYMO), and aluminum(III) *sec*-butoxide. Prehydrolysis of the inorganic precursors leads to sol nanoparticles that are mixed with the block copolymer from organic solvents upon evaporation of all volatiles. Dipole−dipole interactions and hydrogen bonding drive the mixing of the nanoparticles and PEO. While these enthalpic contributions are necessary, they are not sufficient to ensure successful and selective mixing. In addition, the sol prepared from the metal alkoxides has to consist of nanoparticles with small sizes in comparison to the root-mean-square end-to-end distance of the PEO chains so that they can swell the PEO without significantly perturbing polymer chain conformations.[15] Meeting both the enthalpic and the entropic requirements allows for high nanoparticle loadings in the PEO block ("the dense nanoparticle regime")[14] to generate a well-defined two-domain system with the interface between the PI block and the PEO/inorganic domains being distinct.[16] Finally, the low glass transition temperatures of both polymer blocks ensure short structural relaxation times facilitating efficient self-assembly of the nanostructured organic−inorganic composites with high periodic order before the system freezes into the glassy network state of the inorganic domain.[4] All these contributions together make the entire block copolymer phase space experimentally accessible for the present block copolymer−aluminosilicate nanoparticle composites.

The paper is structured as follows. First, synthesis details and preparation protocols for the various materials are given. This is followed by a description of all composite structures with emphasis on bicontinuous cubic structure formation. Details of the structural assignments with the help of combinations of small-angle X-ray scattering (SAXS) and transmission electron microscopy (TEM) investigations were reported in previous publications as indicated in the text below. For brevity their discussion is thus omitted, and only results are summarized for the various composites. Additional TEM investigations are discussed in the context of composites exhibiting biphasic behavior. Differential scanning calorimetry (DSC) studies are then presented to elucidate the role of PEO crystallization in nanocomposites with low inorganic content. All the data are finally summarized by mapping the morphology space in a two-component and a three-component morphology diagram, respectively.

Table 1. Characterization Results of Poly(isoprene-*b*-ethylene oxide) (PI-*b*-PEO) Block Copolymers

polymer	M_n (g/mol)	f_w PEO	f_v PEO[a]	M_w/M_n
P1	84100	0.08	0.07	1.05
P2	14200	0.13	0.11	1.06
P3	19300	0.15	0.13	1.06
P4	16700	0.19	0.16	1.05
P5	14100	0.21	0.18	1.04
P6	38700	0.32	0.28	1.05
P7	16400	0.38	0.33	1.07
P8	10700	0.40	0.35	1.05
P9	23600	0.54	0.49	1.04
P10	30300	0.66	0.60	1.12
P11	44300	0.71	0.67	1.05
P12	26400	0.82	0.79	1.11

[a] Based on a density of 0.91 and 1.12 g/cm^3 for PI and PEO, respectively.[18,19]

Experimental Section

Block Copolymer Synthesis and Hybrid Synthesis. The PI-*b*-PEO block copolymers were polymerized by anionic polymerization as described elsewhere.[17] Gel permeation chromatography (GPC) was used to determine the molecular weight of the first blocks (polyisoprene, PI) and the polydispersity of the block copolymers. ^{1}H NMR was used to determine the overall molecular weights of the block copolymers and the microstructure of the PI block. The molecular weights and polydispersities of the resulting 12 PI-*b*-PEO polymers are listed in Table 1. On average 6% of the PI chains was 3,4-polyisoprene and 94% was 1,4-polyisoprene.

The process used to prepare the structured organic−inorganic hybrid materials is shown schematically in Figure 1. In a typical preparation, a prehydrolyzed sol was prepared by mixing 5.3 g of (3-glycidyloxypropyl)trimethoxysilane (GLYMO) and 1.4 g of aluminum(III) *sec*-butoxide (Al(O^{s}Bu)$_3$) (mole ratio of 8:2) and 38 mg of KCl (7.5 wt % with respect to the mass of polymer) in a 100 mL beaker. This mixture was stirred vigorously for 1−2 min at 0 °C before 0.27 g of 0.01 M HCl (15% of the stoichiometric amount required for the complete hydrolysis of the metal alkoxide groups) was added. After 15 min of stirring the sol at 0 °C, followed by another 15 min at room temperature, 1.7 g of 0.01 M HCl (the residual amount for complete hydrolysis with a 25% molar excess) was added, and the mixture was stirred for another 20 min. Thereafter the required amount of this mixture was filtered through a 0.2 μm PTFE filter and added to the block copolymer solution. This block copolymer solution consisted of 0.5 g of PI-*b*-PEO dissolved in a 1:1 mixture of chloroform and THF by weight (5 wt % polymer solution). The resulting mixture was stirred for another hour before being transferred to a glass Petri dish (5 cm diameter) where it was held at 50 °C. Films were cast beneath a crystallization dish. Heating was controlled using a IKA RET control visc IKA-MAG digital hot plate. After evaporation of the solvents over

(12) Montalvo, G.; Rodenas, E.; Valiente, M. *J. Colloid Interface Sci.* **1998**, *202*, 232–237.
(13) Lipic, P. M.; Bates, F. S.; Hillmyer, M. A. *J. Am. Chem. Soc.* **1998**, *120*, 8963–8970.
(14) Jain, A.; Wiesner, U. *Macromolecules* **2004**, *37*, 5665–5670.
(15) Warren, S. C.; Disalvo, F. J.; Wiesner, U. *Nat. Mater.* **2007**, *6*, 156–161.
(16) De Paul, S. M.; Zwanziger, J. W.; Ulrich, R.; Wiesner, U.; Spiess, H. W. *J. Am. Chem. Soc.* **1999**, *121*, 5727–5736.
(17) Allgaier, J.; Poppe, A.; Willner, L.; Richter, D. *Macromolecules* **1997**, *30*, 1582–1586.

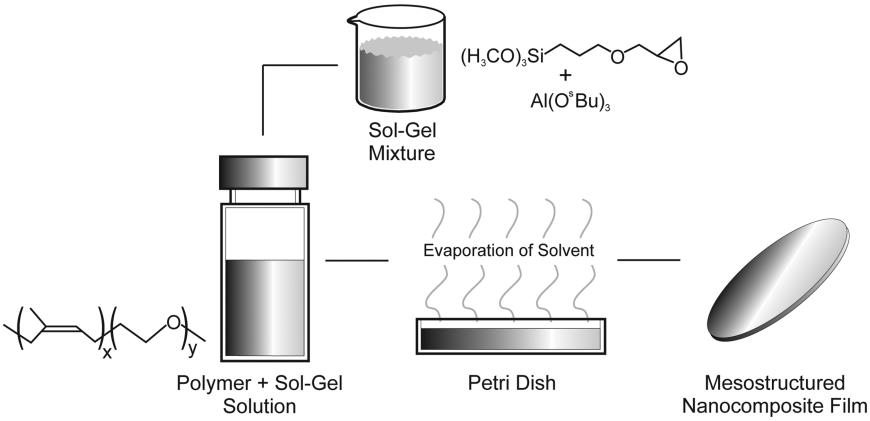

Figure 1. Schematic of the procedure for nanocomposite preparation. A mixture of the prehydrolyzed sol−gel precursors (sol) is added to the polymer solution from which a film is cast in a Petri dish. The final composites are formed by evaporation of all volatiles and subsequent heat treatments as described in the text.

2−3 h at 50 °C, an additional heat treatment followed at 130 °C under vacuum for 1 h. It was found that after this heat treatment typically only 53% of the mass of the sol added to the polymer solution remained in the film. The other 47% mass loss was due to the evaporation of alcohol and water byproducts from the hydrolyzation and condensation reactions. The inorganic weight fractions used for the morphology diagram were based on the amount of inorganic material remaining after the heat treatments. The thickness of the cast films was in the range of 0.5−1 mm.

Gel Permeation Chromatography (GPC). Measurements were performed in 98% tetrahydrofuran (THF) and 2% *N*,*N*-dimethylacetamide at room temperature using 5 μm Waters Styragel columns (10^3, 10^4, 10^5, 10^6 Å, 30 cm each; Waters Corporation, Milford, MA) at a flow rate of 1.0 mL/min. A Waters 490 programmable multiwavelength UV diode array detector (operated at $\lambda = 260$ nm) and a Waters 410 RI detector operated at 25 °C were used. Raw data were processed using PSS-Win GPC V6.2 software (Polymer Standards Service, Mainz, Germany). Molecular weights (M_n) and polydispersity index (M_w/M_n) were calculated using a polyisoprene calibration curve.

^{1}H Nuclear Magnetic Resonance (NMR). ^{1}H solution NMR spectra were recorded on a Varian INOVA 400 MHz spectrometer using $CDCl_3$ signal ($\delta = 7.27$ ppm) as an internal standard.

Transmission Electron Microscopy (TEM). Ultrathin sections (thickness 30−100 nm) were produced with a Leica Ultracut UCT microtome at −55 °C. Sample slices were collected on a water/DMSO solution and transferred to 300 mesh copper grids. To prepare isolated nanoparticles for TEM imaging a 0.05 wt % colloidal solution was prepared by dissolving a piece of the composite film in cyclohexane and stirring for 2−3 days followed by probe sonication. A 5 μL drop of this solution was placed on a carbon coated grid, and the solvent was evaporated. This procedure is only valid for composites where the PEO−aluminosilicate phase does not form a continuous domain. TEM was performed on a Leo 912 W (tungsten filament) operated at 120 kV with an objective aperture angle of 16.5 mrad.

Small-Angle X-ray Scattering (SAXS). SAXS data were obtained on a Bruker-AXS Nanostar and on a Rigaku RU300. The Nanostar consisted of an X-ray source (Cu Kα, $\lambda = 1.54$ Å) operated at 40 kV and 40 mA. Göbel mirrors were used to focus the beam. A 2-D Hi-Star area detector at a sample-to-detector distance of 62.5 cm was used to record the scattering images. The Rigaku RU300 setup consisted of a copper rotating anode X-ray spectrometer ($\lambda = 1.54$ Å) operated at 40 kV and 50 mA. X-rays were monochromated with a Ni filter and focused by orthogonal Franks mirror optics. SAXS patterns were imaged with a home-built 1000 × 1000 pixel CCD detector.[20] The distance from the sample to detector and position of the beam center were determined using a silver behenate ($d_{lamellar} = 5.8376$ nm) calibrant.

Differential Scanning Calorimetry (DSC). DSC was performed on hybrids with a TA Instruments Q1000 DSC, calibrated with an indium standard. Measurements were taken on heating from −80 to 100 °C at 10 °C/min, without prior annealing of the samples.

Results and Discussion

We investigated the composition space of 64 different organic−inorganic nanocomposites derived from 12 different polymers of varying molecular weight and PEO fraction (see Table 1) and varying aluminosilicate content (see Table 2). All hybrids were prepared under identical conditions (see Experimental Section) and were transparent, suggesting the lack of macroscopic phase separation between the aluminosilicate and block copolymer, which was corroborated by TEM investigations (data not shown). Macroscopic segregation is prevented by strong interactions between the PEO block and the small aluminosilicate nanoparticles. The compositions of each of the nanocomposites listed in Table 2 are based on both the volume fraction of the PEO−inorganic domain and the weight fraction of each component in the composite. The PEO−inorganic mixture is considered a single domain based on the results of a previous solid state NMR study on the nature of the interface between polyisoprene (PI) and PEO−inorganic domains. Spin diffusion measurements demonstrated that no relevant interphase (< 1 nm) of pure PEO exists between the PI and PEO−aluminosilicate type domains for the compositions

(18) Finnefrock, A. C.; Ulrich, R.; Du Chesne, A.; Honeker, C. C.; Schumacher, K.; Unger, K. K.; Gruner, S. M.; Wiesner, U. *Angew. Chem., Int. Ed.* **2001**, *40*, 1207–1211.
(19) Floudas, G.; Vazaiou, B.; Schipper, F.; Ulrich, R.; Wiesner, U.; Iatrou, H.; Hadjichristidis, N. *Macromolecules* **2001**, *34*, 2947–2957.
(20) Tate, M. W.; Gruner, S. M.; Eikenberry, E. F. *Rev. Sci. Instrum.* **1997**, *68*, 47.

Table 2. Sample Descriptions

composite	vol. fraction[a] PEO−inorganic	wt fraction PI	wt fraction PEO	wt fraction[b] inorganic	morphology[c]
P1-1	0.27	0.64	0.06	0.30	Cyl
P1-2	0.29	0.62	0.05	0.33	Cyl
P1-3	0.34	0.55	0.05	0.40	Cyl + Lam
P1-4	0.60	0.30	0.03	0.67	Lam + InvCyl
P1-5	0.67	0.24	0.02	0.74	InvCyl
P2-1	0.23	0.69	0.10	0.21	Sph
P2-2	0.25	0.67	0.10	0.23	Sph + Cyl
P2-3	0.28	0.63	0.09	0.28	Cyl
P2-4	0.31	0.60	0.09	0.31	Cyl
P2-5	0.34	0.56	0.08	0.36	Cyl + Lam
P2-6	0.45	0.43	0.07	0.50	Lam
P2-7	0.50	0.40	0.06	0.54	Lam
P2-8	0.55	0.35	0.05	0.60	Lam
P2-9	0.66	0.24	0.04	0.72	InvCyl
P2-10	0.70	0.22	0.03	0.75	InvCyl
P2-11	0.71	0.21	0.03	0.76	InvCyl
P2-12	0.73	0.19	0.03	0.78	InvCyl
P2-13	0.76	0.17	0.03	0.80	InvCyl
P2-14	0.85	0.11	0.02	0.87	WM
P3-1	0.36	0.54	0.10	0.36	PN
P3-2	0.36	0.54	0.09	0.37	PN
P3-3	0.52	0.37	0.07	0.56	Lam
P3-4	0.61	0.27	0.05	0.68	Lam + InvCyl
P3-5	0.66	0.25	0.04	0.71	InvCyl
P3-6	0.76	0.17	0.03	0.80	InvCyl
P4-1[d]	0.24	0.67	0.16	0.17	Sph + Cyl
P4-2	0.34	0.55	0.13	0.32	Cyl + Lam
P4-3	0.62	0.28	0.07	0.65	Lam + InvCyl
P5-1[d]	0.25	0.66	0.18	0.16	Sph + Cyl
P5-2[d]	0.27	0.63	0.17	0.20	Cyl
P5-3[d]	0.29	0.61	0.16	0.23	Cyl
P5-4	0.44	0.45	0.12	0.43	Lam
P5-5	0.67	0.25	0.07	0.68	InvCyl
P5-6	0.82	0.12	0.03	0.85	InvSph
P6-1[d]	0.39	0.50	0.24	0.26	Lam
P6-2	0.63	0.28	0.12	0.60	InvCyl
P7-1	0.57	0.33	0.20	0.47	Lam
P7-2	0.61	0.30	0.18	0.52	Lam + InvCyl
P7-3	0.64	0.27	0.15	0.58	InvG
P7-4	0.65	0.26	0.14	0.60	InvG
P7-5	0.73	0.19	0.12	0.69	InvCyl
P7-6	0.76	0.17	0.10	0.73	InvCyl
P7-7	0.83	0.12	0.07	0.81	InvSph
P8-1[d]	0.40	0.50	0.33	0.17	Lam
P8-2	0.50	0.40	0.26	0.34	Lam
P8-3	0.56	0.34	0.23	0.43	Lam
P8-4	0.61	0.30	0.20	0.50	Lam + InvCyl
P8-5	0.62	0.28	0.19	0.53	Lam + InvCyl
P8-6	0.64	0.26	0.18	0.56	InvCyl
P8-7	0.65	0.26	0.17	0.57	InvCyl
P8-8	0.66	0.25	0.17	0.58	InvCyl
P9-1[d]	0.53	0.36	0.43	0.21	Lam
P9-2[d]	0.59	0.31	0.37	0.32	Lam
P9-3	0.64	0.27	0.32	0.41	InvCyl
P9-4	0.83	0.12	0.14	0.74	InvSph
P10-1	0.82	0.12	0.24	0.64	InvSph
P10-2	0.86	0.10	0.19	0.71	InvSph
P11-1[d]	0.73	0.20	0.48	0.32	InvCyl
P11-2[d]	0.76	0.17	0.42	0.41	InvCyl
P11-3	0.89	0.07	0.18	0.75	InvSph
P12-1	0.88	0.08	0.38	0.54	InvSph
P12-2	0.89	0.07	0.34	0.59	InvSph
P12-3	0.92	0.06	0.25	0.69	InvSph
P12-4	0.95	0.04	0.16	0.80	InvSph

[a] Volume fraction calculated from an experimentally determined value of 1.4 g/cm^3 for the density of the PEO−inorganic phase and 0.91 g/cm^3 for the PI phase.[4] [b] Weight fraction based on 53% of the original mass of the aluminosilicate sol mixture added to the polymer. [c] Structure determined from a combination of SAXS and TEM data. [d] Samples show evidence of PEO crystallization in DSC.

studied.[16] The results revealed that the PEO is completely integrated within the aluminosilicate type network resulting in a quasi-two domain system with PI and PEO−inorganic domains.

Morphological Behavior. Morphological behavior was analyzed using a combination of small-angle X-ray scattering (SAXS) and transmission electron microscopy (TEM) as described, for example, in refs 4 and 21. The

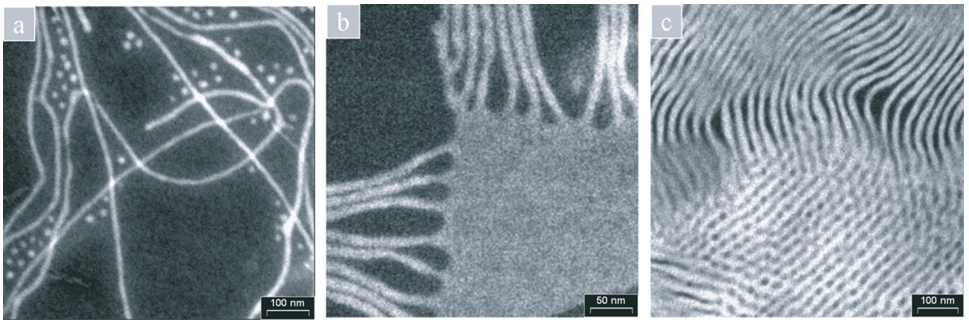

Figure 2. TEM images of samples P2-2 (a), P2-5 (b), and P3-4 (c) demonstrating the biphasic character of the composites in the respective composition ranges. Samples P2-2 and P2-5 were prepared by dissolution of the composites in cyclohexane and subsequent placement on a TEM grid. Sample P3-4 was microtomed and then imaged.

identified composite morphologies are the sphere (Sph, PEO−inorganic spheres in a PI matrix), the hexagonal cylinder (Cyl, PEO−inorganic cylinders in a PI matrix), the Plumber's Nightmare (PN, 3-D cubic bicontinuous PEO−inorganic channels in a PI matrix), the lamellar (Lam, PEO−inorganic layers alternating with PI layers), the inverse double gyroid (invG, 3-D cubic bicontinuous PI channels in a PEO−inorganic matrix), the inverse hexagonal cylinder (invCyl, PI cylinders in a PEO−inorganic matrix), the worm-like micelle (WM, PI worms in a PEO−inorganic matrix), and inverse sphere (invSph, PI spheres in a PEO−inorganic matrix) structures.

Bicontinuous Network Structures. For specific PEO−nanoparticle volume fractions using polymers P3 and P7, a bicontinuous network structure was observed. As recently reported, the combined data from SAXS and TEM from hybrids with a PEO−aluminosilicate *majority* volume fraction of 0.64 (hybrids P7-3 and P7-4) are most consistent with a uniaxially compressed double gyroid morphology.[21] This double gyroid morphology is the predicted and observed morphology for pure block copolymers in this volume fraction regime. In contrast, hybrids with a PEO−aluminosilicate *minority* volume fraction of 0.36 (hybrids P3-1 and P3-2) showed SAXS data that are not consistent with a gyroid but instead are more consistent with a Plumber's Nightmare (PN) structure.[22] For the thorough structure analysis of these bicontinuous network composites the interested reader is referred to the respective literature.[18,21−23] A possible explanation for why two different morphologies are observed is that the aluminosilicate nanoparticles can stabilize the sixfold node of the Plumber's Nightmare structure. In hybrids with a PEO−aluminosilicate *majority* volume fraction, filling the center of the nodes in the PN phase requires significant stretching of the polyisoprene chains resulting in an elastic contribution to the free energy. Since the double gyroid only has threefold nodes, filling the center of the nodes requires less polymer chain stretching, thus rendering the double gyroid thermodynamically more stable than the PN structure. For hybrids with a PEO−aluminosilicate minority volume fraction, through a heterogeneous composition distribution within the channels, the nanoparticles can fill the center area of the PN node, thus allowing the polymer chains to relax into a lower energy conformation. The explanation is consistent with the observation of the gyroid morphology in the Pluronics/TEOS system for which the silica/EO domains form the majority volume fraction while the hydrophobic blocks form the minority channels.[24,25] This situation can also be compared to that encountered in studies of homopolymer mixed with one phase of a block copolymer. Like nanoparticles, a homopolymer can also

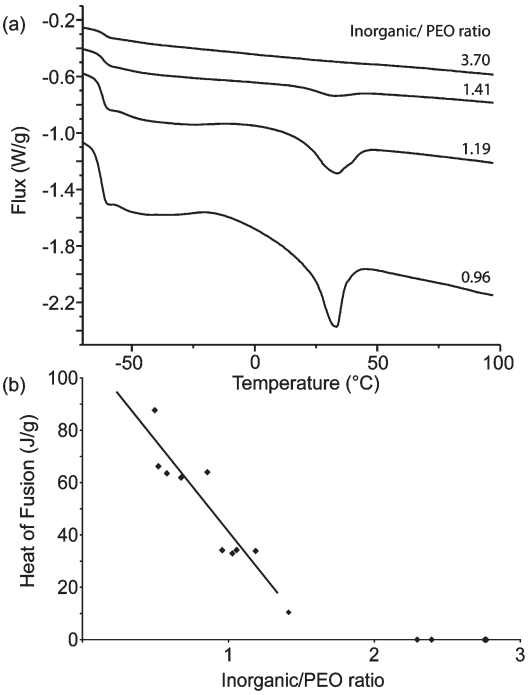

Figure 3. Heating cycles of DSC thermograms for inorganic/PEO weight ratios of 3.70, 1.41, 1.19, and 0.96 (a). Plot of the heat of fusion of PEO versus inorganic/PEO weight ratio indicating that PEO crystallization is completely suppressed at inorganic/PEO weight ratios larger than 1.3−1.5 (b). The line in (b) is drawn as a guide for the eye.

(21) Toombes, G. E. S.; Finnefrock, A. C.; Tate, M. W.; Ulrich, R.; Wiesner, U.; Gruner, S. M. *Macromolecules* **2007**, *40*, 8974–8982.
(22) Jain, A.; Toombes, G. E. S.; Hall, L. M.; Mahajan, S.; Garcia, C. B. W.; Probst, W.; Gruner, S. M.; Wiesner, U. *Angew. Chem., Int. Ed.* **2005**, *44*, 1226–1229.
(23) Finnefrock, A. C.; Ulrich, R.; Toombes, G. E. S.; Gruner, S. M.; Wiesner, U. *J. Am. Chem. Soc.* **2003**, *125*, 13084–13093.
(24) Liu, X.; Tian, B.; Yu, C.; Gao, F.; Xie, S.; Tu, B.; Che, R.; Peng, L.-M.; Zhao, D. *Angew. Chem., Int. Ed.* **2002**, *41*, 3876.
(25) Tian, B.; Liu, X.; Solovyov, L. A.; Liu, Z.; Yang, H.; Zhang, Z.; Xie, S.; Zhang, F.; Tu, B.; Yu, C.; Terasaki, O.; Zhao, D. *J. Am. Chem. Soc.* **2004**, *126*, 865–875.

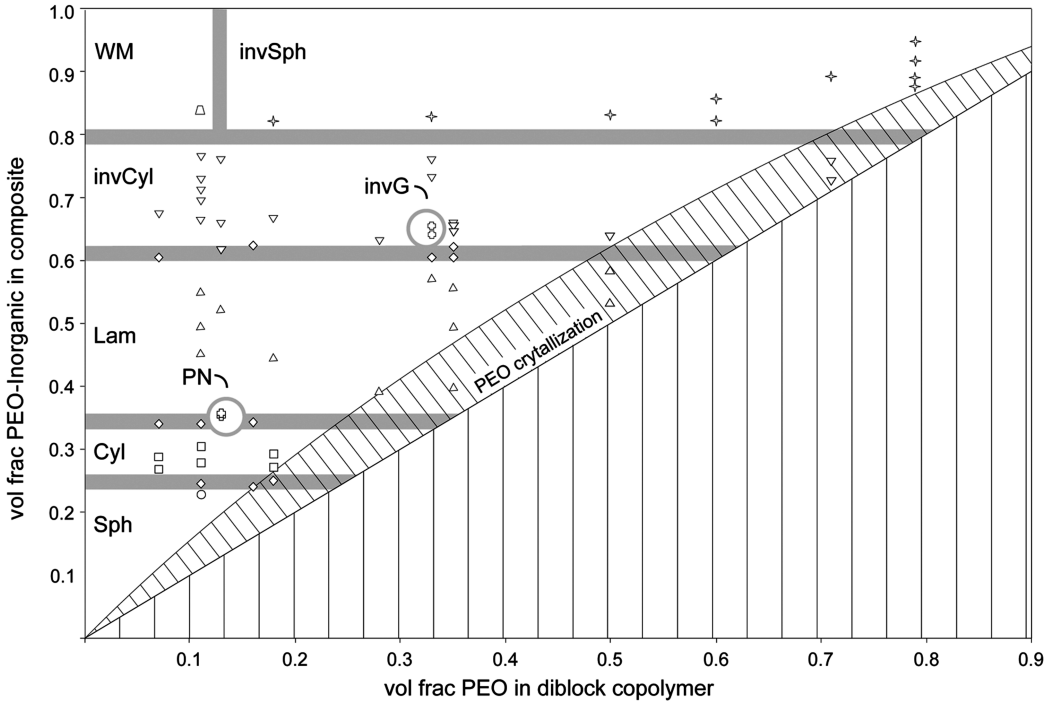

Figure 4. Given a diblock copolymer with a certain PEO volume fraction, this diagram displays the data points in Table 2 using the volume fraction of PEO−inorganic domains in the composites. The gray bars across the diagram roughly indicate regions where biphasic composites are observed/expected. The region hatched with diagonal lines represents the composition of composites where PEO crystallization is observed. The curved boundary line of this region represents composites where the inorganic:PEO weight ratio is equal to 1.5 above which PEO crystallization is completely suppressed.

preferentially concentrate inside the nodes,[26] thereby stabilizing the gyroid and other bicontinuous phases.[27] Recent lattice Monte Carlo (MC) simulations predicted a mesophase progression from gyroid to double diamond (DD) to PN upon increasing homopolymer concentration in a gyroid-forming block copolymer melt.[28] Furthermore, a combination of particle-based simulations and self-consistent field theory (SCFT) was used to study the stability of bicontinuous phases in these block copolymer/homopolymer blends with respect to macrophase separation. It was shown that although the PN phase was always metastable, the regions were located significantly far from the spinodal line, suggesting that this phase could be very long-lived and would probably get "trapped" once formed.[29]

Biphasic Behavior. TEM was the primary means to identify composites with biphasic character. Composites exhibiting biphasic behavior are highlighted in Table 2 by indicating the two coexisting morphologies observed in the sample. For composites with continuous PI domains, biphasic behavior is revealed by imaging isolated nanoparticles obtained through dissolution of the bulk film (see Experimental Section). Figure 2 shows representative TEM micrographs of sample P2-2 with coexisting spherical and hexagonal cylindrical structures (Figure 2a), sample P2-5 with coexisting hexagonal cylindrical and lamellar structures (Figure 2b), and sample P3-4 with coexisting lamellar and inverse hexagonal cylindrical structures (Figure 2c). Figure 2b obtained after film dissolution shows cylinders growing out of the plane of an individual lamellar sheet like fingers growing out of a hand. Figure 2c obtained from a microtomed specimen depicts vertically oriented lamellar sheets which merge with a region showing an inverse hexagonal cylindrical structure. These composites all have compositions that indeed place them at the interface between neighboring morphology regions in the morphology diagrams as depicted in Figures 4 and 5 below. Biphasic regions are predicted in theory for block copolymer−homopolymer mixtures[30] in accordance with Gibb's phase rule, $F = C - P + 2$, where two degrees of freedom, F, are expected for a two-component system, C, and two phases, P, resulting in a finite area where two morphologies can coexist thermodynamically. These regions have also been observed experimentally in block copolymer−epoxy blends.[13] It should be emphasized that we cannot say for sure that the composites represent thermodynamic equilibrium structures due to the short time scale on which the structure is set from cross-linking of the hybrid-aluminosilicate matrix. Films are cast by evaporation of the solvent over a period of 2−3 h after which the structure is set by the inorganic network formation. This may not be enough time to allow the structure to adopt the most thermodynamically stable state. It should also be noted that polymer and nanoparticle systems always have some polydispersity,

(26) Hasegawa, H.; Hashimoto, T.; Hyde, S. T. *Polymer* **1996**, *37*, 3825–3833.
(27) Matsen, M. W.; Bates, F. S. *Macromolecules* **1996**, *29*, 7641–7644.
(28) Martinez-Veracoechea, F. J.; Escobedo, F. A. *Macromolecules* **2007**, *40*, 7354–7365.
(29) Martinez-Veracoechea, F. J.; Escobedo, F. A. *Macromolecules* **2009**, *42*, 1775–1784.
(30) Likhtman, A. E.; Semenov, A. N. *Macromolecules* **1997**, *30*, 7273–7278.

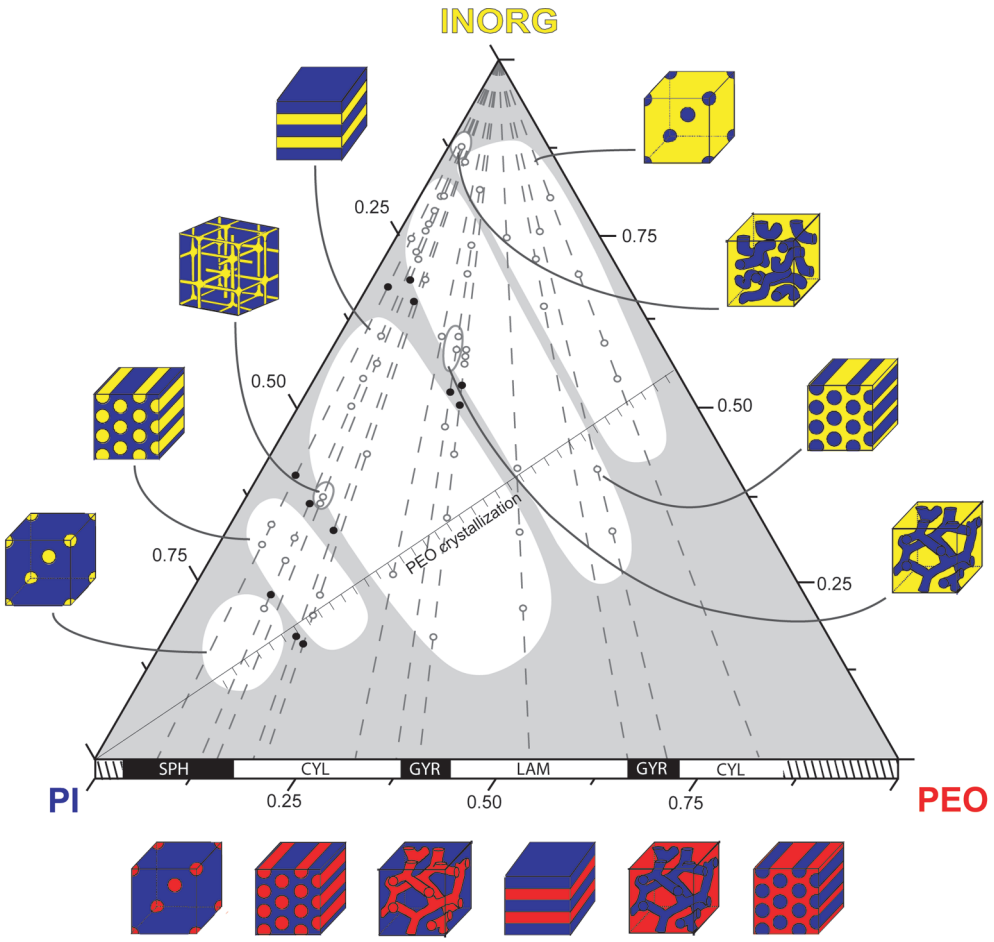

Figure 5. Ternary diagram mapping out the morphologies found for various compositions (in weight fractions) of the system PI-*b*-PEO plus aluminosilicate sol nanoparticles derived from (3-glycidyloxypropyl)trimethoxysilane (GLYMO) and aluminum(III) *sec*-butoxide ($Al(O^sBu)_3$). At the bottom of the diagram are shown schematics of the morphologies found for the pure PI-*b*-PEO diblock copolymer. Hatched areas along the PI-PEO axis indicate areas where no data was available from the diblock copolymer diagram in ref. 19. Each white region within the diagram is labeled with a schematic representing the morphology of the composites formed. The yellow (light) regions in these schematic morphologies on the right and left are a representation of the PEO + inorganic domains. Closed dark points on a gray background indicate areas where biphasic behavior is observed.

which may blur the sharpness of nominally first order phase boundaries. The observed sequence of morphologies and quality of structure formation do suggest, however, that the system is certainly not far from equilibrium.

PEO Crystallinity. The pure PI-*b*-PEO block copolymer system shows different morphological behavior than that found for the present polymer−inorganic composites. At low temperatures (below ~50 °C), upon PEO crystallization, most phases revert to the crystalline lamellar morphology.[19] Only for very low PEO volume fractions the segregation strength between PI and PEO is sufficiently strong to confine crystallization within the microphase separated PEO domains. For all other PEO weight fractions the crystalline lamellar morphology is observed at lower temperatures. The SAXS data of the PI-*b*-PEO/aluminosilicate hybrids does not follow this trend, suggesting that the hybrid-aluminosilicate nanoparticle network suppresses PEO crystallization. Differential scanning calorimetry (DSC) measurements, see Figure 3, were performed to check for PEO crystallization in the hybrids. Only composites with a low inorganic/PEO ratio (by weight) showed an endothermic peak upon heating associated with the melting of crystalline PEO (Figure 3a). Figure 3b presents the heat of fusion versus the inorganic/PEO weight ratio for 13 nanocomposites. The plot shows that composites with an inorganic/PEO ratio of less than 1.3−1.5 are semicrystalline. The actual density of the crystalline PEO−inorganic domains may be higher than that of the amorphous region, resulting in a slight error in the actual volume fraction of the two-component domains. Composites found in this regime are indicated with an asterisk in Table 2. The weight fractions of each of the components are also calculated and tabulated so that two morphology maps can be constructed (see below): one based on the PEO−aluminosilicate volume fraction and a second one (a ternary diagram) based on the PI, PEO, and organically modified aluminosilicate weight fractions.

Two-Component Morphology Diagram. The data collected on all composite samples are summarized in two morphology maps. The first is based on the two-domain concept (PI and PEO−aluminosilicate domains, respectively) of the composites. In Figure 4 the PEO volume fraction in the diblock copolymer is plotted along the abscissa and the volume fraction of the PEO−inorganic domain in the composite along the ordinate. The

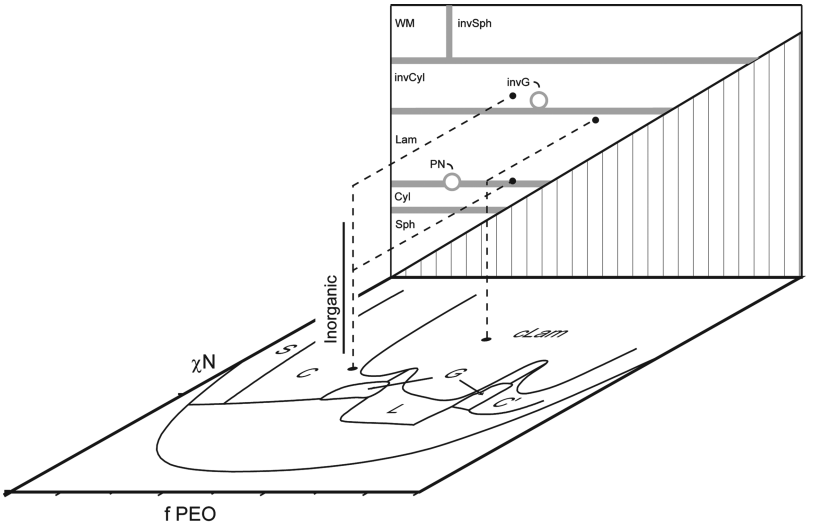

Figure 6. Composites used in this study prepared from block copolymers with varying χN values. Results are projected onto a single plane to map the morphology diagram. The $x-y$ plane represents the PI-*b*-PEO phase diagram[19] while the $x-z$ plane represents the projected hybrid morphology diagram of Figure 4.

hatched-line region labeled "PEO crystallization" indicates that a fraction of the PEO in the composites found in this region will crystallize. The degree of crystallization would be inversely proportional to the amount of inorganic in the composites, and crystallization is completely suppressed beyond an inorganic/PEO weight fraction ratio of 1.3−1.5 (see previous section). Gray regions separating composites with well-defined structures indicate regions where biphasic behavior was observed or is expected. The composition ranges for which bicontinuous structures were discovered are small and located between the hexagonal cylinder and lamellar structures. This is consistent with the morphological behavior found in pure diblock copolymers. From looking at the two-component morphology diagram in Figure 4 it is evident that by adding increasing amounts of the inorganic components, block copolymers like P2 and P7 show up to five and four different well-defined composite morphologies, respectively. This nicely demonstrates the versatility of the present approach.

Three-Component Morphology Diagram. A ternary composition map based on the weight fraction of each component (PI, PEO, and aluminosilicate) is shown in Figure 5 summarizing the location of the composite structures observed in the PI-*b*-PEO/aluminosilicate system. In this diagram, the dashed lines represent the 12 block copolymers and their compositions used in preparation of the composites. These lines converge on the inorganic vertex since the polymer composition does not change with the addition of inorganic material. The structures of the bulk diblock copolymers according to the PI-*b*-PEO phase diagram at a value of $\chi N = 50$ are represented by a schematic at the bottom of the diagram.[19] Open points representing compositions showing a particular morphology have been encircled in a white background and are identified by a schematic of that morphology on the left and right sides of the diagram. Note that these white areas serve as a guide for the eye for regions of well-defined morphology. The results of studies of over 60 polymer−inorganic nanocomposites are summarized in this ternary diagram that exhibits eight distinct morphologies: the sphere, the hexagonal cylinder, the Plumber's Nightmare, the lamellar, the inverse double gyroid, the inverse hexagonal cylinder, the worm-like micelle, and inverse sphere structures. Closed, dark points in areas depicted in a light gray and found outside the circled white areas represent composites with biphasic character. The morphology of these composites is determined by a combination of the morphologies adjacent to the point. The solid line converging on the PI vertex roughly indicates the onset of PEO crystallization in the composites for compositions below this line (for details, see Table 2). Although some samples have been prepared and analyzed, this region remains essentially unexplored. Nonetheless, to the best of our knowledge, this is the first time that results of such a comprehensive morphological investigation of block copolymer-aluminosilicate composite structures are reported.

High Dimensional Morphology Diagrams. An important factor that is not considered in this investigation is the influence of the parameter, χN, usually used to describe morphological behavior of block copolymers. This would require either a systematic preparation of block copolymers with increasing PEO fraction at a constant χN value and their composites or the mapping of the full three-dimensional parameter space as indicated in Figure 6. Rather, the composites prepared in this study were made from a variety of block copolymers with χN values ranging from 60 to 400 (χN values for polymers used in this study were calculated using $\chi = 65/T + 0.125$, see ref 19). Figure 6 demonstrates how the morphology diagrams presented in this paper are the projection of morphological data points onto a single plane. The result is an average over a large parameter space thereby neglecting the influence of χN on the morphology of the polymer−inorganic composites. As an example, it is quite

possible that the bicontinuous structures observed in the present composites are sensitive to the χN of the block copolymer. Future studies are needed to elucidate this behavior in more detail.

Conclusions

We have investigated the compositional space of organic−inorganic hybrid materials obtained from the amphiphilic diblock copolymer PI-*b*-PEO as the structure directing agent for aluminosilicate nanoparticles. Careful analysis of compositions with low inorganic content reveals the existence of crystalline PEO while all other compositions are all-amorphous. Results are constituted in two morphology diagrams including biphasic regions found at the interface between composition regions of well-defined morphologies. Although thermodynamic equilibrium may not be possible in the present system due to cross-linking of the inorganic matrix over a 2−3 h time period, the sequence of eight well-defined morphologies and the quality of the observed structure formation suggest at least close proximity to equilibrium. Since the properties of organic−inorganic hybrid materials are strongly dependent on their structure, these morphology maps may serve as a guide for interesting future structure−property correlation studies.[31] This is particularly relevant for energy conversion and storage applications where block copolymer directed structure formation of inorganic materials may play an important role for the improvement of device performance.[32−34]

Acknowledgment. The financial support of the Gates Millennium Fellowship, the National Science Foundation (award DMR-0605856), and U.S. Department of Energy (BER Grant DE-FG02-97ER62443) is gratefully acknowledged. The work was further supported by the Cornell Center for Materials Research (CCMR), a Materials Research Science and Engineering Center of the National Science Foundation (DMR-0520404).

(31) Verploegen, E.; Dworken, B. T.; Faught, M.; Kamperman, M.; Zhang, Y. M.; Wiesner, U. *Macromol. Rapid Commun.* **2007**, *28*, 572–578.
(32) Cho, B.-K.; Jain, A.; Gruner, S. M.; Wiesner, U. *Science* **2004**, *305*, 1598–1601.
(33) Crossland, E. J. W.; Kamperman, M.; Nedelcu, M.; Ducati, C.; Wiesner, U.; Smilgies, D. -M.; Toombes, G. E. S.; Hillmyer, M. A.; Ludwigs, S.; Steiner, U.; Snaith, H. J. *Nano Lett.* **2009**, *9*, 2807–2812.
(34) Orilall, M. C.; Matsumoto, F.; Zhou, Q.; Sai, H.; Abruna, H.; Disalvo, F.; Wiesner, U. *J. Am. Chem. Soc.* **2009**, *131*(26), 9389–9395.